Galloping of steepled main cables in long-span suspension bridges during construction

Yonghui An[1a], Chaoqun Wang[2b], Shengli Li[*2] and Dongwei Wang[2c]

[1]*Department of Civil Engineering, State Key Laboratory of Coastal and Offshore Engineering, State Key Laboratory of Structural Analyses for Industrial Equipment, Dalian University of technology, Dalian, China*
[2]*School of Civil Engineering, Zhengzhou University, Zhengzhou, China*

Abstract. Large amplitude oscillation of steepled main cables usually presents during construction of a long-span bridge. To study this phenomenon, six typical main cables with different cross sections during construction are investigated. Two main foci have been conducted. Firstly, aerodynamic coefficients of a main cable are obtained and compared through simulation and wind tunnel test: (1) to ensure the simulation accuracy, influences of the numerical model's grid size, and the jaggy edges of main cable's cross section on main cable's aerodynamic coefficients are investigated; (2) aerodynamic coefficients of main cables at different wind attack angles are obtained based on the wind tunnel test in which the experimental model is made by rigid plastic using the 3D Printing Technology; (3) then numerical results are compared with wind tunnel test results, and they are in good agreement. Secondly, aerodynamic coefficients of the six main cables at different wind attack angles are obtained through numerical simulation. Then Den Hartog criterion is used to analyze the transverse galloping of main cables during construction. Results show all the six main cables may undergo galloping, which may be an important reason for the large amplitude oscillation of steepled main cables during construction. The flow structures around the main cables indicate that the characteristic of the airflow trajectory over a steepled main cable may play an important role in the galloping generation. Engineers should take some effective measures to control this harmful phenomenon due to the big possibility of the onset of galloping during the construction period.

Keywords: main cable; galloping; wind tunnel test; suspension bridge; construction period

1. Introduction

Large-scale bridges play an important role in modern economies (An, Spencer *et al.* 2015), and structural safety is a major concern for the public (An, Bartlomiej *et al.* 2016). The wind effects on bridges are more obvious with the increase in the bridge span (Wang, Li *et al.* 2011, Wang, Li *et al.* 2013). The main cables of a long-span suspension bridge usually show hexagon cross section after

---

∗Corresponding author, Associate Professor, E-mail: lsl2009@126.com
[a] Associate Professor, Email: anyh@dlut.edu.cn
[b] Master Student, Email: wcqoffice@163.com
[c] Professor, Email: dongweiwang@zzu.edu.cn

construction; generally, there are two methods to conduct the construction of the main cables: the steepled main cables (Li and Ou 2009) in which two edges of the hexagon cross section are vertical, and the flat-topped main cables in which two edges of the hexagon cross section are horizontal. Researchers have found that steepled main cables of long-span suspension bridges can suffer galloping, which can seriously affect the safety and progress of construction during the construction period (Li and Ou 2009). Galloping is a relevant issue during both the design and the construction stages of engineering structures. Galloping is a type of crosswind vibration that often occurs in slender structures with non-circular section shapes, for example, the inclined square prism (Hu, Tse *et al*. 2015a, Tse, Hu *et al*. 2014), the iced conductor (Den Hartog 1932), and the main cable during construction (Li and Ou 2009). When wind speed reaches a critical value, the effects of negative aerodynamic damping counteract the effects of inherent damping on the structure; the structure thus continually absorbs energy from the wind field (Den Hartog 1932). Therefore, the amplitude of galloping is characterized as unstable. In addition, the amplitude of galloping is usually very large, and it can lead to structural damage or failure (Wang 1996).

Den Hartog (1932), one of the pioneers in the field, established a criterion based on quasi-steady theory when studying the transverse galloping of the iced transmission line, which can be used to predict whether a structure has the potential to gallop. Then, researchers have conducted a series of studies on the onset of galloping in various types of engineering structures based on the classical criterion (Li and Ou 2009, Cai, Yan *et al*. 2015). Further researches have been conducted to study the amplitude of galloping, and efficient control measures have been proposed. Hu et al. (2012) first obtained the aerodynamic coefficients of the iced conductor by wind tunnel test and then studied the galloping amplitude of various types of iced conductors via time histories analysis based on the obtained aerodynamic coefficients. Furthermore, Yan, Hu *et al*. (2011) invented a damper that could control the transverse galloping of the iced conductor.

The aerodynamic characteristics of slender structures have been found to play an important role in the onset and the amplitude of galloping, and the aerodynamic characteristics greatly depend on the cross-sectional shape of the slender structures (Cai, Yan *et al*. 2015). The influences of changing the cross-sectional shape on the galloping performances of slender structures have been widely investigated (Ibarra, Sorribes *et al*. 2014). For example, a D-section prism with the circular surface facing the flow condition cannot gallop in any flow condition (Païdoussis, Price *et al*. 2010). For a circular cylinder fitted with a splitter plate, the galloping response varies with the different shapes of the splitter plate (Assi and Bearman 2015). Accurate aerodynamic coefficients of one slender structure at different wind attack angles are the key parameters for examining galloping (Macdonald and Larose 2007). In general, researchers obtained the aerodynamic coefficients through the wind tunnel test (Hu, Tse *et al*. 2015b, Xin, Li *et al*. 2012), numerical simulation (Li, Wang *et al*. 2015b, Rezvani and Mohebbi 2014), or the combination of the two methods (Defraeye *et al*. 2010).

Li and Ou (2009) obtained the aerodynamic coefficients of steepled main cables for long-span suspension bridges using a simple model based on the Computational Fluid Dynamics (CFD) simulation and predicted whether the main cable in different construction periods has the potential to gallop. In engineering, the cross-sections of the main cables during the construction period have jaggy edges, which were ignored in the study of Li and Ou (2009). However, the numerical result may be significantly influenced by the grid size of the numerical model (Blocken and Toparlar 2015). Thus, the numerical model must be optimized to ensure the accuracy and the reliability of the aerodynamic coefficients. Furthermore, it is important to conduct the corresponding wind tunnel test for further validation.

The purpose of the present paper is to investigate the galloping of steepled main cables in different construction periods more accurately. Both the CFD simulations and wind tunnel tests have been conducted. First, the aerodynamic coefficients of one main cable at different wind attack angles are obtained on the basis of the wind tunnel test. Then, to ensure the accuracy of the results, the influences of the numerical model's grid size and the jaggy edges of the main cable's cross section on the numerical result are studied. The numerical results are compared with the experimental results. Finally, the transverse galloping of the main cables during construction are studied by the CFD simulation based on the Den Hartog criterion.

2. Models and theory

2.1 Models

The research objects in this paper are based on the design parameters of the Xihoumen Bridge, which has a main span of 1650 m and has been observed to undergo large amplitude oscillation during the construction of the main cables. Fig. 1 illustrates the designed cross-section of the main cable (Li and Ou 2009); the numbers in the figure indicate the construction sequence of the 169 steel ropes. To investigate the galloping of the main cable in different construction periods, six cables that refer to six typical construction periods (Fig. 2) are selected as research objects. The cable's six cross-sections are named main cables 1# to 6#, respectively, as shown in Fig. 2.
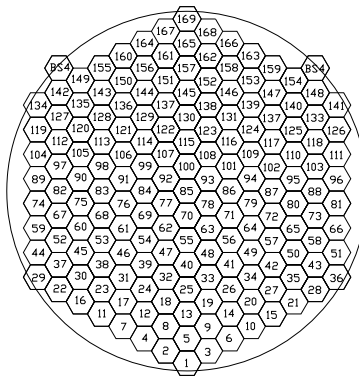

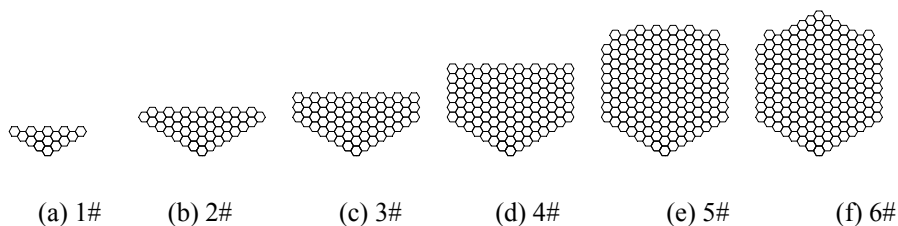Fig. 1 The designed cross-section of the steepled main cable

(a) 1#   (b) 2#   (c) 3#   (d) 4#   (e) 5#   (f) 6#

Fig. 2 Main cables referring to the six typical construction periods in this work
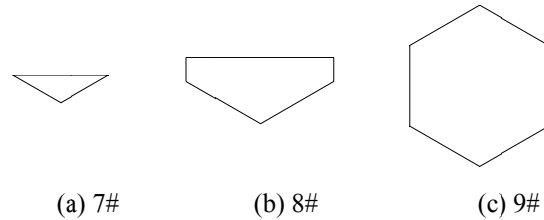
(a) 7#   (b) 8#   (c) 9#

Fig. 3 Simplified models of the main cable in different construction periods

Considering the complexity of meshing and the convergence rate in numerical simulation, geometry models are usually simplified in previous studies (Li and Ou 2009). However, the ignored jaggy edges of the main cable's cross section may affect the accuracy of the numerical results. To address this problem, three simplified models (Fig. 3) denoted as main cables 7#, 8#, and 9#, which correspond to the main cables 1#, 3#, and 6# in Fig. 2, are adopted for comparison. The nine models mentioned above are investigated by the same numerical simulation method in the following pages.

2.2 Theory of galloping analysis

Generally, aerodynamic forces can be defined in two ways as shown in Fig. 4. F_D and F_L are the drag force and lift force in the wind axes, respectively; F_H and F_V are the drag force and lift force in the body-axis coordinate system, respectively; and α is the wind attack angle, which ranges from -5° to 5° with an interval of 1° in this study.

For a two-dimensional model of the main cable, the aerodynamic coefficients mainly depend on its cross-section shape. The lift force and drag force are defined as follows
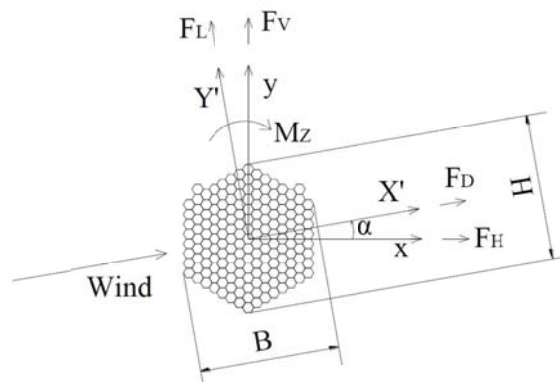
$$C_D = \frac{F_D}{\frac{1}{2}\rho U^2 HL} \tag{1}$$
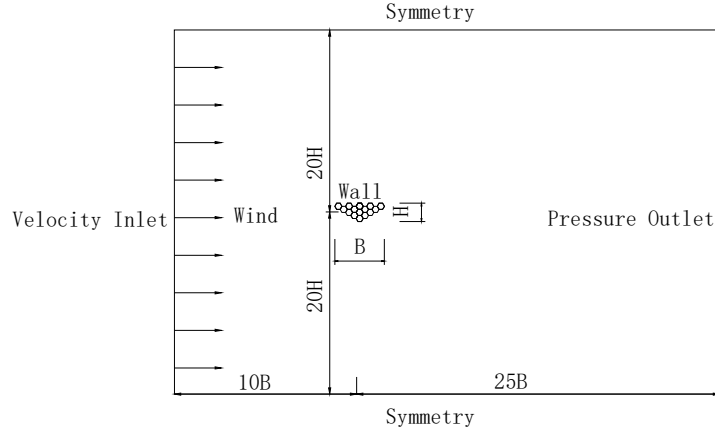

Fig. 4 Forces on the main cable

Fig. 5 Numerical model of the main cable 1#

$$C_{\mathrm{L}} = \frac{F_{\mathrm{L}}}{\dfrac{1}{2}\rho U^2 BL} \qquad (2)$$

where ρ is the air density and it is 1.225 kg/m^3, U is the wind velocity and it is 10 m/s, and H and B are the cable's height and width in the wind axes, respectively (Fig. 4).

The classical criterion established by Den Hartog (1932) is adopted to study the onset of galloping in this paper. The criterion indicates that galloping may occur when the aerodynamic characteristic of a slender structure meets the following formula

$$A = \frac{\partial C_{\mathrm{L}}}{\partial \alpha} + C_{\mathrm{D}} < 0 \qquad (3)$$

where *A is* the Den Hartog coefficient.

3. Comparison between the experiment and the numerical simulation

To ensure accuracy of the numerical results, the influences of the numerical model's grid size, and the jaggy edges of the main cable's cross section on the main cable's aerodynamic coefficients are investigated. The aerodynamic coefficients of main cable 1# are obtained based on the numerical simulation and the wind tunnel test, respectively, for comparison.

3.1 Numerical simulation

A 2D numerical model is established in the CFD software ANSYS FLUENT to obtain the aerodynamic coefficients of the main cable 1#. To maintain consistency, the scale ratio of the

model and the wind speed are the same as those in the wind tunnel test. The computational domain and boundary conditions in the numerical model are determined as shown in Fig. 5. With consideration of computation time and accuracy, a high resolution of grids is used in the boundary-layer region as shown in Fig. 6. The grids close to the main cable are quadrilateral cells which are very small, and the periphery grids in the computational domain are also quadrilateral cells. As is known, quadrilateral cells have greater advantages than those of triangular cells in calculation accuracy in the region close to the wall. Meanwhile, in consideration of the complicated shape of the main cable's cross-section, triangular cells are used between the periphery grids and the internal grids close to the main cable (Fig. 6(b)).
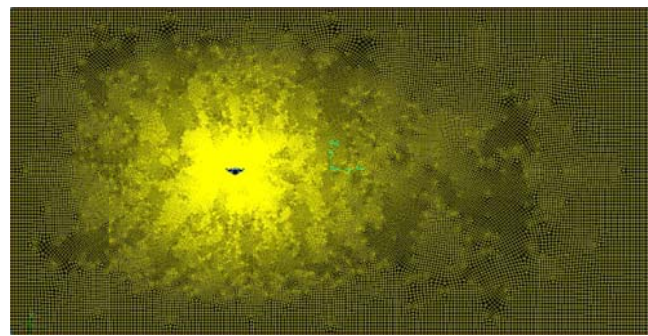
(a) Grids in the computational domain
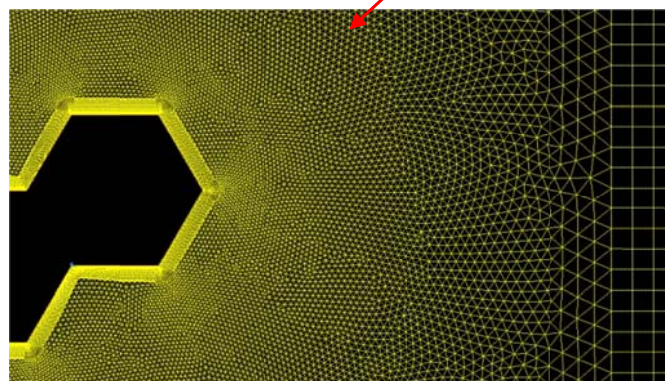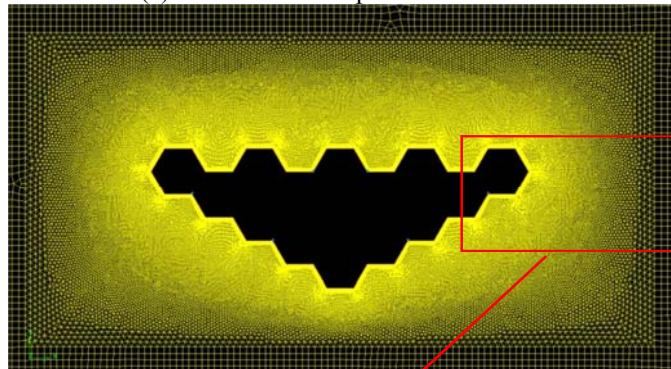
(b) Computational grids near the main cable 1#

Fig. 6 Mesh view

(a) $y^+ < 90$ (b) $y^+ < 35$ (c) $y^+ < 13$

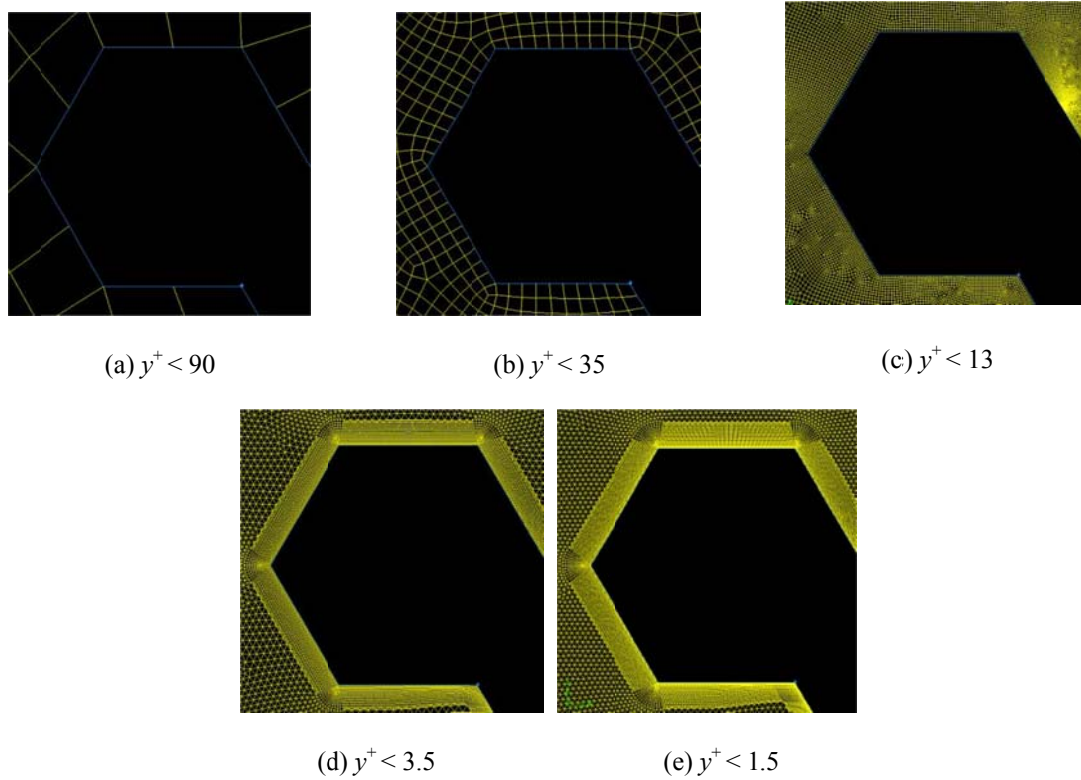(d) $y^+ < 3.5$ (e) $y^+ < 1.5$

Fig. 7 Close-up views of the mesh near the main cable 1#

The Reynolds numbers of the numerical models for the six main cables 1#~6# are in the range of 3.1×10^4~1.52×10^5, which fall into the turbulent flow regime. The turbulent intensities in numerical models are in the range of 3.5%~4.5%, which are determined by the Reynolds numbers. The equations RANS (Reynolds Averaged Navier-Stokes) are chosen and solved with the SST k-ω model (Li, Wang *et al.* 2015a). Pressure-velocity coupling is taken care of by the SIMPLEC algorithm, and the second order interpolation is used in the calculation of the pressure.

Grid size in the boundary-layer region significantly affects the numerical results (Franke, Hellsten *et al.* 2007). Furthermore, a dimensionless parameter y^+ is commonly used for the size of the grids in the boundary-layer region (Blocken and Toparlar 2015). y^+ is defined as follow

$$y^+ = \frac{\Delta y}{v} \sqrt{\frac{\tau_w}{\rho}} \tag{4}$$

where Δy is the distance from the wall to the center of a grid adjacent to the wall; v is the kinematic viscosity; τ_w is the wall shear stress; ρ is the air density.

Thus, a grid-sensitivity analysis based on y^+ is conducted to ensure computational accuracy. Five numerical models with different values of y^+ are adopted to compute the aerodynamic coefficients of the main cable 1# under the wind attack angles 0° and ±5°. Fig. 7 indicates the close-up views of the mesh near the main cable 1# (Fig. 6) for the five numerical models. The results are presented in Fig. 8.

(a)   (b)
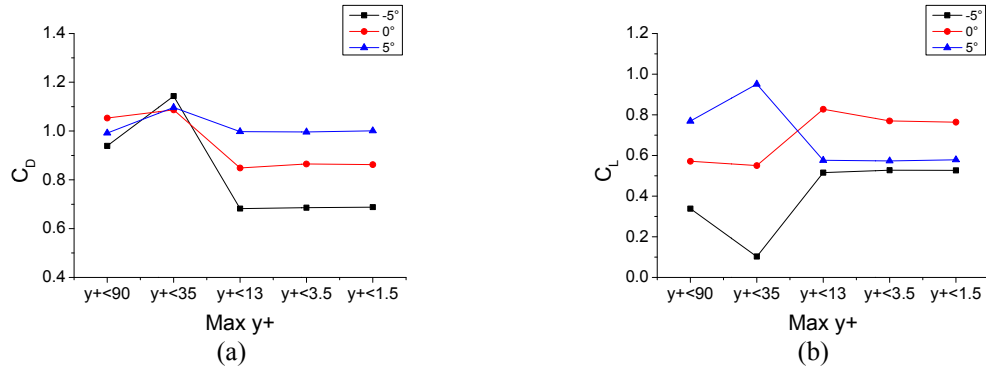
Fig. 8 Results of the five models with different values of y^+
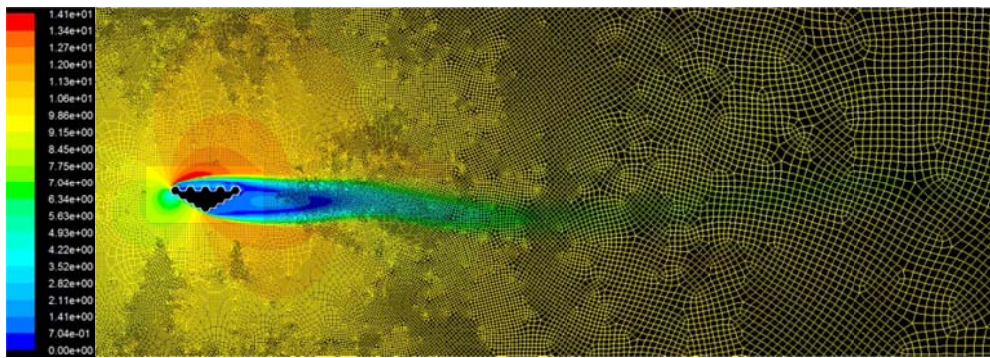
Fig. 9 Velocity contours of the model for main cable 1# under the 0° wind attack angle

The figure indicates that the aerodynamic coefficients of main cable 1# at different wind attack angles vary with the value of y^+ ranging from 90 to 3.5, and then they almost remain a constant with the value of y^+ ranging from 3.5 to 1.5. In theory, the result becomes more accurate with the reduction of the grid size. The result can be considered converged when the value of y^+ is reduced to 3.5. Thus, the value of y^+ is set to 3.5 in the following numerical simulation. The wake structure of the model under the 0° wind attack angle for a converged simulation with $y^+ = 3.5$ is shown by the velocity contours (Fig. 9).

To study the effect of the jaggy edges of the main cable's cross section on the numerical result, main cable models 1#, 3#, and 6#, as well as the three corresponding simplified models 7#, 8#, 9#, are selected for comparison. Their aerodynamic coefficients are shown in Figs. 10-12. According to these figures, the aerodynamic coefficients (Fig. 10) of main cables 1# and 7# agree well with each other. As for main cables 3# and 8#, their lift coefficients agree well with each other, but at the wind attack angles from -3° to 0°, the trends of drag coefficients (Fig. 11) are variable. The drag coefficients (Fig. 12) of main cables 6# and 9# agree well with each other, but obvious differences occur in the lift coefficients. To sum up, there is influence of the jaggy edges of the main cable's cross section on numerical results. Based on the Den Hartog criterion, the influence cannot be ignored in the study of the onset of galloping.
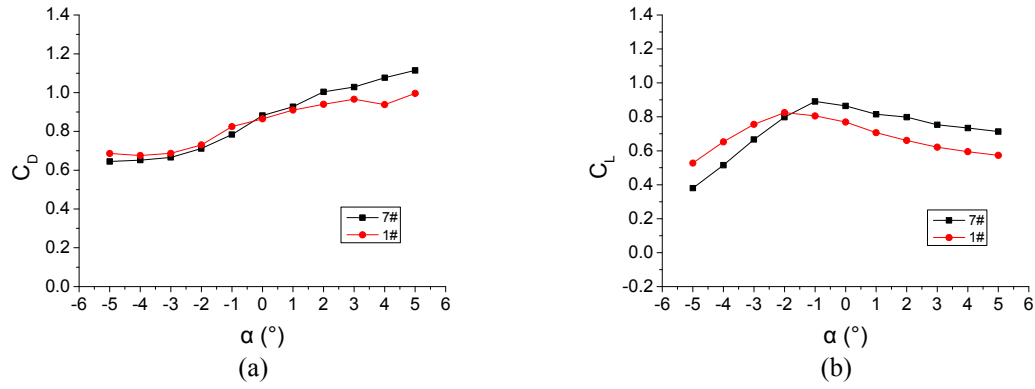
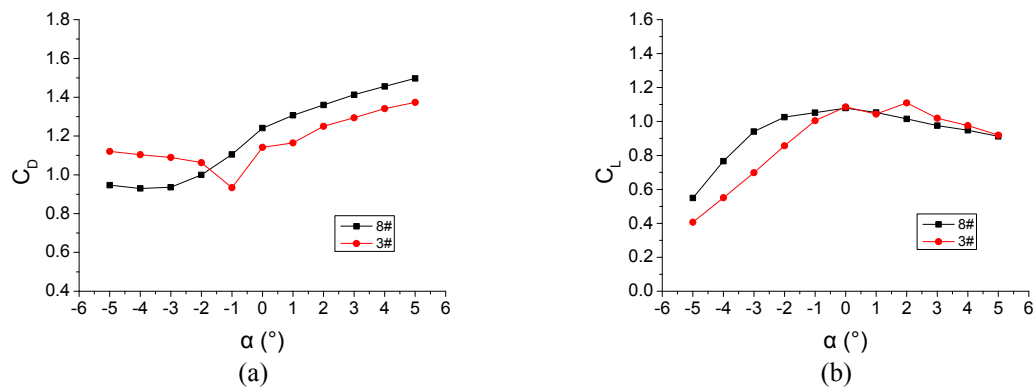Fig. 10 Aerodynamic coefficients of main cables 1# and 7#

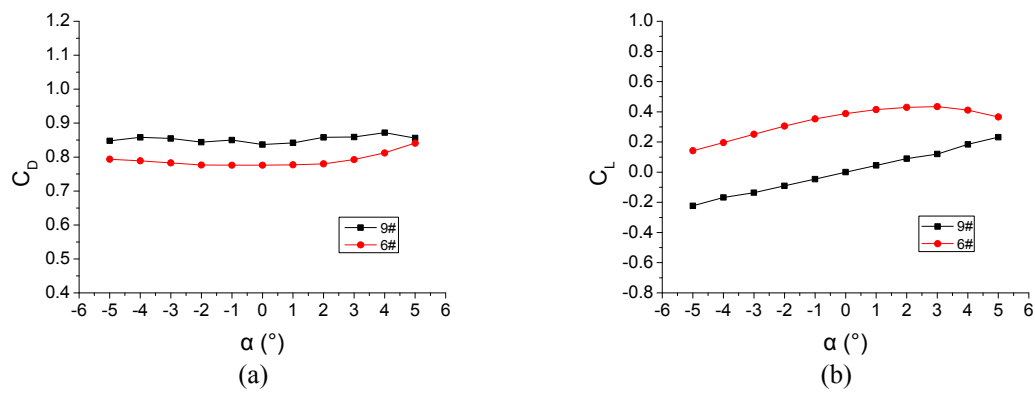Fig. 11 Aerodynamic coefficients of main cables 3# and 8#

Fig. 12 Aerodynamic coefficients of main cables 6# and 9#

Table 1 Dimension parameters of the experimental model

Parameter	Value
Scale Ratio	1:4
Length L (mm)	1000
Width B (mm)	120
Height H (mm)	45.5
Length-width ratio	8.33

3.2 Experiment

The wind tunnel test was conducted in the high-speed test section of the DUT-1 wind tunnel at the Dalian University of Technology, China. The size of the wind tunnel test section is 18 m×3 m×2.5 m (length × width × height). To ensure the quantity of the wind flow, the distance between the experimental model and the wind inlet is 2/3 of the length of the test section. The turbulent intensity is no more than 0.8% in the wind tunnel. Tests are performed under a quasi-laminar flow in the rear part of the test section, and the wind attack angles range from -5° to 5° with an interval of 1°. The blockage ratio of the model in the wind tunnel is approximately 1.6%, which is much lower than the critical value of 5% (Holmes 2015). The speed inhomogeneity of the flow field in the wind tunnel is no more than 1.0% (accounting for more than 75% of the total deck section area), the directional inhomogeneity is no more than 1°, and the average flow direction is no more than 1°. The flow quality is high. The Reynolds number of the main cable model is the same with the corresponding numerical model. Considering the complex shape of the cross-section, the experimental model is made using 3D printing technology with rigid plastic. The dimension parameters of the experimental model are determined as shown in Table 1.

Forces are measured by a high-frequency force balance equipped on the bottom board of the wind tunnel, and the sampling frequency and duration are 100 Hz and 40 s, respectively. The test wind speed is 10 m/s. To reduce the effect due to the upper end, a rectangular plate is hung over the model as shown in Fig. 13. The feature dimensions of the end plate (Fig. 13) are about 10 times of those of the model cross-section to avoid three-dimensional effects at the tip of the model. The plate should be horizontally hung over the model and very close to the model top. In addition, the wind speeds of 10 m/s, 13.8 m/s and 15 m/s are adopted to conduct the wind tunnel test, and the test results based on the three wind speeds are very close. Thus, the test results on the Reynolds number in this study are dependable. The depth of wall boundary layer in the cross-section of the wind tunnel has been taken into account in the test. Many experiments for models with different cross-sections have been conducted to study the influence of the wall boundary layer on the measured forces of the model. Results indicate that for such a model with a constant section and a length of 1m, the forces measured by the balance should be multiplied by a reduction factor of 0.9; and the forces have been multiplied by such a reduction factor in this paper.
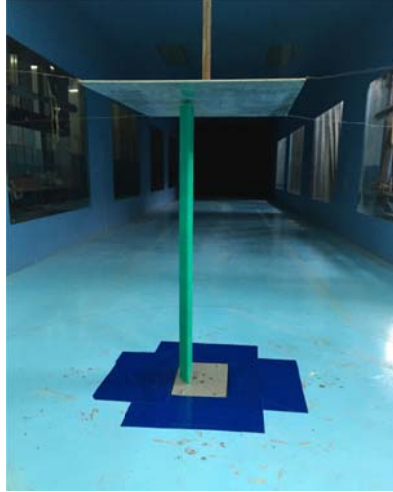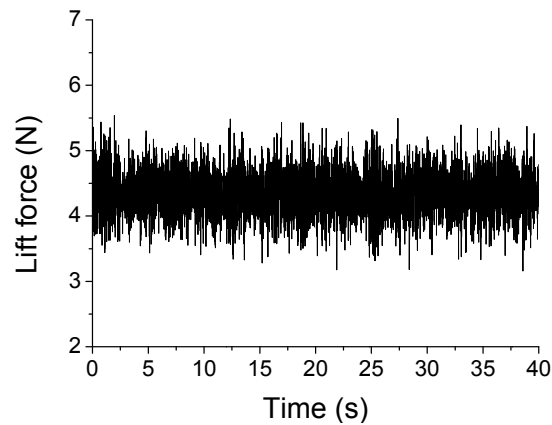
Fig. 13 Experimental model in the wind tunnel

Fig. 14 Time history of lift force for the experimental model ($\alpha = 0°$)

Take the test results at the wind attack angle of 0° for example, the time history of lift force and the corresponding amplitude spectrum are shown in Figs. 14 and 15, respectively. There are three main frequencies in Fig. 15. The predominant frequency is 41.77 Hz, and the corresponding Strouhal number of the test model is 0.186.

3.3 Comparison of the results

The aerodynamic coefficients of main cable 1# at the wind attack angles of -5° to 5° are obtained by the two methods described above, respectively, as shown in Fig. 16. All the differences in the drag coefficients determined by the two methods are less than 0.2; the trends of

drag coefficients, determined by the two methods, are highly close. The lift coefficients determined by the two methods are very close at the wind attack angles from 0° to 5° but show some differences at the wind attack angles from -5° to 0°. In general, the results using the two methods are different, and the possible reasons for the differences are listed as follows:

(1) The main cable is an ideal 2D model in the numerical simulation. Although there are two end plates placed at the two ends of the model, respectively, the three-dimensional effects are just minimized but they still exist. So the approximate 2D experimental model is still different from the 2D numerical model.

(2) Although the forces measured by the balance have been multiplied by a reduction factor, the wall boundary layer in the cross-section of the wind tunnel may affect the test results to some extent.

(3) The airflow is turbulent in the numerical model but laminar in the wind tunnel.

(4) The main cable has a smooth surface in the numerical model but a rough surface in the test.

The Den Hartog criterion indicates that galloping occurs when the trend of lift coefficients goes downward. Thus, the prediction of whether galloping occurs or not is consistent based on the two methods. The studies on the onset of galloping by the two methods reach the same conclusion.
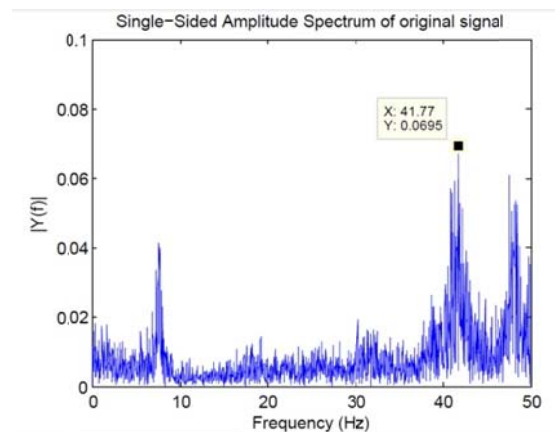

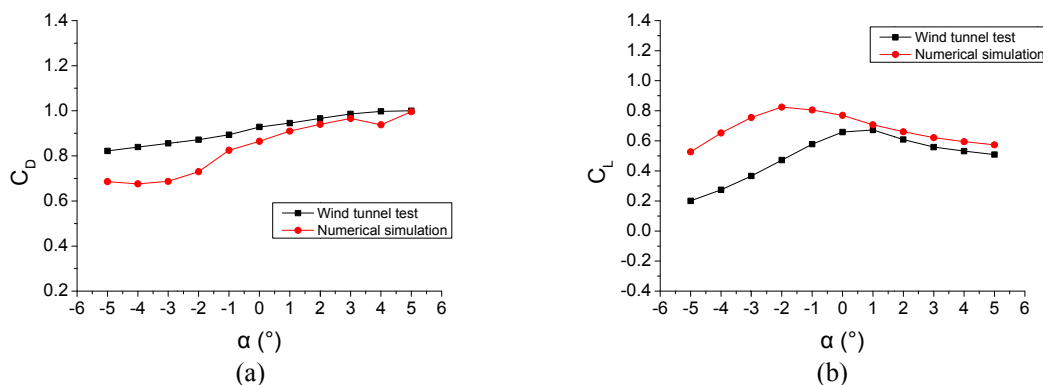Fig. 15 Amplitude spectrum of the lift force time history for the experimental model ($\alpha = 0°$)

Fig. 16 Aerodynamic coefficients of main cable 1# based on wind tunnel test and numerical simulation
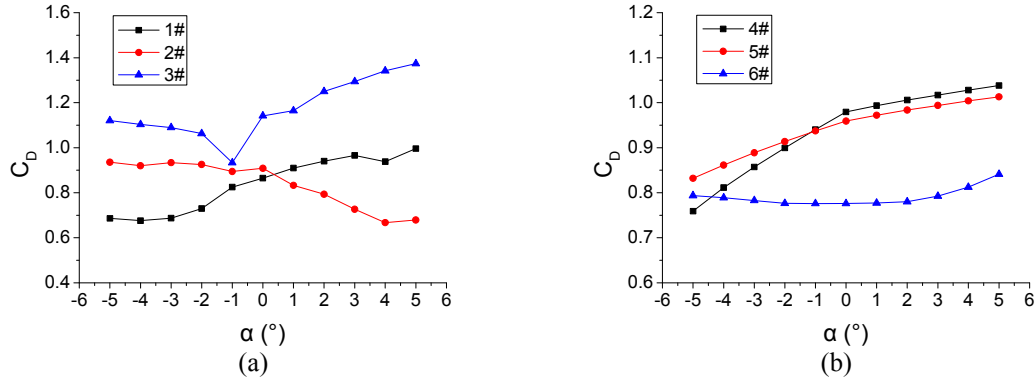
Fig. 17 Drag coefficients of the main cables with consideration of the jaggy edges of main cables' cross sections
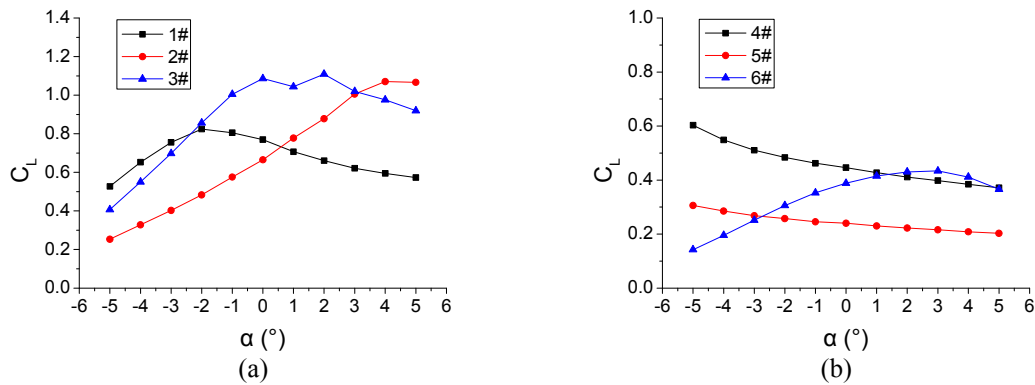

Fig. 18 Lift coefficients of the main cables with consideration of the jaggy edges of main cables' cross sections

4. Galloping analysis

The comparison above shows that both wind tunnel test and numerical simulation can be used to study the galloping of main cables. With consideration of the high cost of the wind tunnel test, the aerodynamic coefficients of main cables 1#~6# are determined by numerical simulation as shown in Figs. 17 and 18. The results show that aerodynamic coefficients of the main cable vary with the progress of the construction. Fig. 18 indicates that the lift coefficients of all the main cables decrease in certain range of the wind attack angles.

The Den Hartog coefficients are obtained by Eq. (3) to predict the onset of galloping. In general, different fitting equations (e.g. polynomials with different orders) can lead to very different results of the Den Hartog coefficient (Pagnini *et al*. 2016, Mannini, Marra *et al*. 2014). In consideration of the potential error caused by the fitting equations, taking main cable 1# for example, polynomials

with different orders are chosen for the fitting of the curves of the force coefficients versus the attack angle (Fig. 19). As for the drag coefficients, Fig. 19 shows that the 7th and 9th order polynomials appear slightly different at the two ends and they are almost overlapped around α = 0°. As for the lift coefficients, the 5th, 7th and 9th order polynomials are almost overlapped. According to Eq. (3), the first derivative of the lift coefficient with respect to the attack angle is very important to the result of Den Hartog coefficient. Fig. 20 shows the derivative of the lift coefficients with respect to the attack angle, and Den Hartog coefficients corresponding to the force coefficient curves fitted by polynomials for main cable 1#. The 5th, 7th and 9th order polynomials appear slightly different around α = 0°, but the 9th order polynomial shows significant difference with the 5th and 7th order polynomials at the two ends. As is known, high order polynomials may lead to very scattered results when fitting a curve if the given sample points are not sufficient, that is why the 9th order polynomial shows significant difference with the 5th and 7th order polynomials at the two ends. In conclusion, the 5th and 7th order polynomials are appropriate for the fitting of the curves of force coefficients versus the attack angles.

(a) Drag coefficients   (b) Lift coefficients

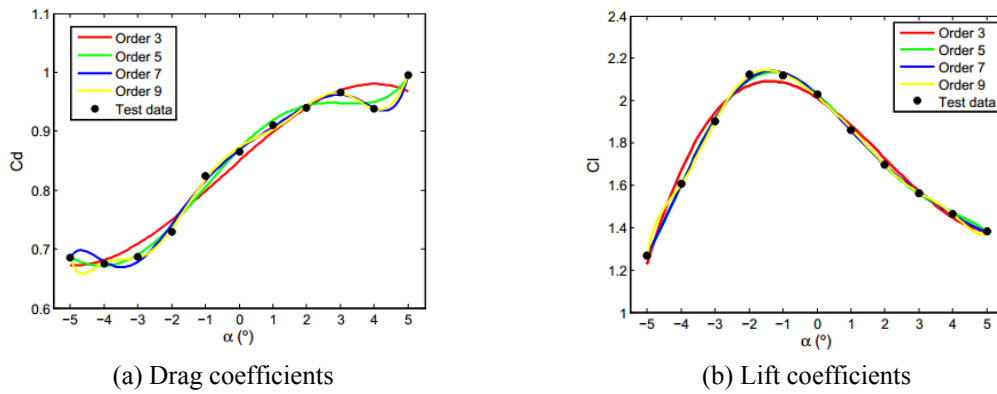Fig. 19 Polynomial fitting of force coefficients using different polynomial orders for main cable 1#

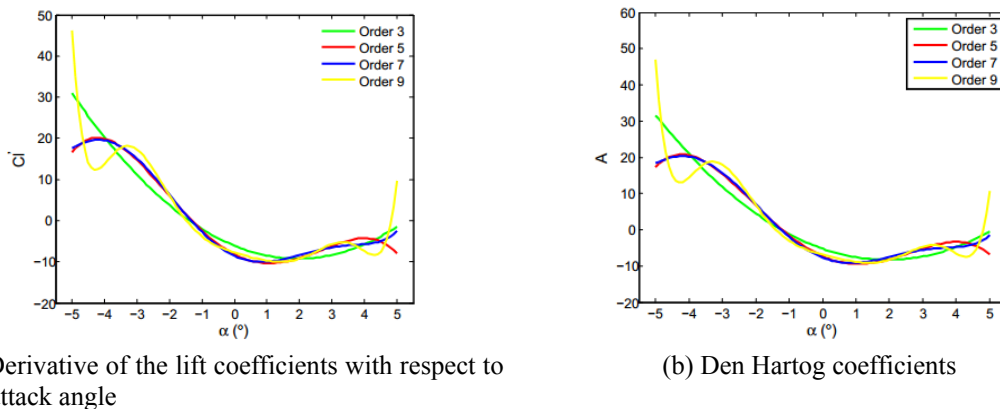(a) Derivative of the lift coefficients with respect to the attack angle   (b) Den Hartog coefficients

Fig. 20 Derivative of the lift coefficients with respect to the attack angle and Den Hartog coefficients corresponding to the force coefficient curves fitted by polynomials for main cable 1#
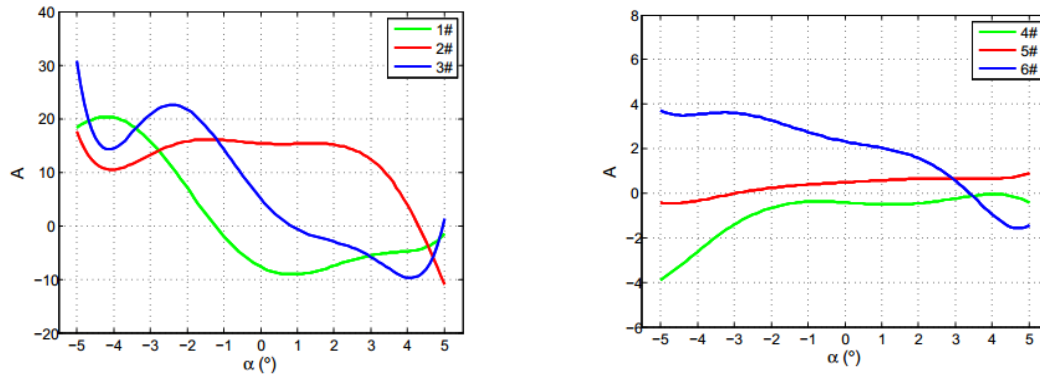
Fig. 21 Den Hartog coefficients corresponding to force coefficient curves fitted by 7th order polynomial for the six main cables

Den Hartog coefficients corresponding to force coefficient curves fitted by 7th order polynomial for the six main cables are shown in Fig. 21. In addition, the main cables with negative Den Hartog coefficients are selected and shown in Table 2. It can be seen form Table 2 that all the main cables have negative Den Hartog coefficients, and this indicates these cables may suffer galloping. The number of wind attack angles that correspond to the negative Den Hartog coefficients presents no obvious trend with the progress of the construction (for comparison, only integers of the wind attack angles are shown). Therefore, there is no obvious difference in the galloping probabilities of different construction stages.

Researchers have investigated the galloping generation mechanism by experiment (Kim and Kim 2014) and simulation (Tang, Zheng *et al.* 2015), and these studies are based on dynamic models or aeroelastic models. In this paper, steady models are adopted in numerical simulation, thus the flows are steady.

Table 2 Cases with negative Den Hartog coefficients

Main cable	Wind attack angles that correspond to the negative Den Hartog coefficients	Number of the wind attack angles that correspond to the negative Den Hartog coefficients
1#	-1°~5°	7
2#	5°	1
3#	1°~4°	4
4#	-5°~5°	11
5#	-5°~-4°	2
6#	4°~5°	2

(a1) 1#, +4°, galloping

(a2) 1#, -4°, no galloping

(b1) 2#, +4°, no galloping

(b2) 2#, -4°, no galloping

(c1) 3#, +4°, galloping

(c2) 3#, -4°, no galloping

(d1) 4#, +4°, galloping

(d2) 4#, -4°, galloping

(e1) 5#, +4°, no galloping

(e2) 5#, -4°, galloping
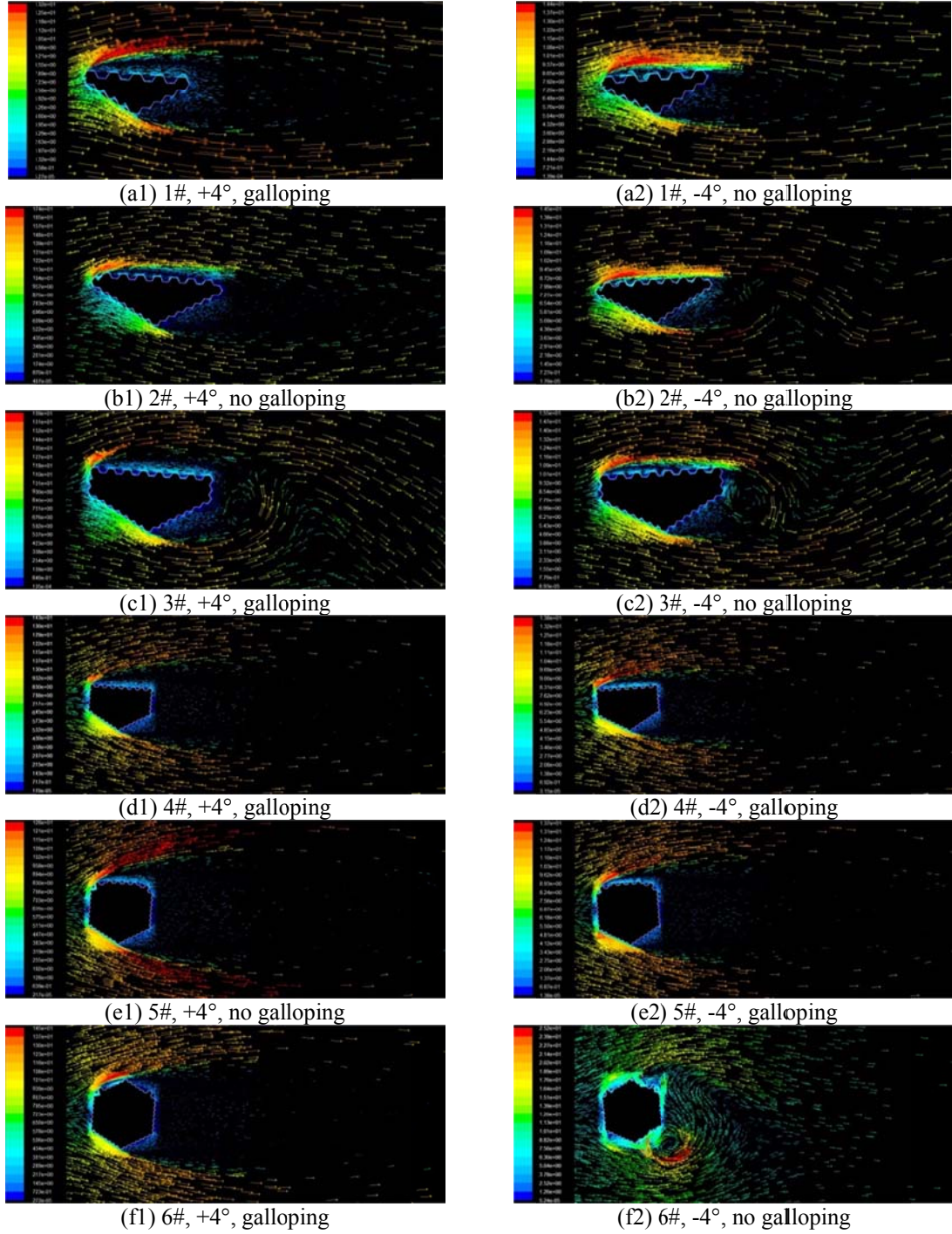
(f1) 6#, +4°, galloping

(f2) 6#, -4°, no galloping

Fig. 22 Velocity vector fields near the six main cables

Table 3 Galloping performances and flow characteristics for main cables 1#~6#

Main cable		Galloping performance	Flow characteristic over the main cable (see Fig. 22)
1#	+4°	galloping	no reattachment
	-4°	no galloping	reattachment
2#	+4°	no galloping	reattachment
	-4°	no galloping	reattachment
3#	+4°	galloping	no reattachment
	-4°	no galloping	reattachment
4#	+4°	galloping	no reattachment
	-4°	galloping	no reattachment
5#	+4°	no galloping	no reattachment
	-4°	galloping	no reattachment
6#	+4°	galloping	no reattachment
	-4°	no galloping	reattachment

As is known, the galloping generation is connected to the fluid dynamics around a model. To study the galloping generation mechanism, the flow structures around the main cables are extracted from the numerical results. For instance, the flow characteristics of the six main cables under the wind attack angles -4° and +4° are presented in terms of a velocity vector fields (Fig. 22). According to Fig. 22, for some cases (e.g., main cable 1# under wind attack angle +4°), the air directly bypass over the main cables at the windward side with no apparent reattachment phenomenon; but for the other cases (e.g., main cable 2# under wind attack angle -4°), the air bypasses over the main cables at the windward side and then reattaches the main cables. Galloping performances and flow characteristics over main cables 1#~6# for the cases in Fig. 22 are shown in Table 3. There is an obvious rule in Table 3: the air bypasses over a main cable at the windward side and then reattaches the main cable if the main cable has the potential to gallop under a wind attack angle, on the contrary, the air directly bypasses over a main cable at the windward side with no apparent reattachment phenomenon if the main cable has no potential to gallop under a wind attack angle. This rule works for almost all the 12 cases (except for main cable 5# under wind attack angle +4°) of the six main cables under the wind attack angles -4° and +4°. The Den Hartog coefficient of main cable 5# under wind attack angle +4° is close to 0. In consideration of calculation error of the Den Hartog coefficient, it seems that the rule mentioned above may reveal the galloping generation mechanism for the steepled main cables. At least, the rule indicates that the characteristic of the airflow trajectory over a steepled main cable may play an important role in the galloping generation of the steepled main cables.

According to Den Hartog criterion, negative aerodynamic damping is a necessary condition for the onset of galloping. When wind speed reaches a critical value, the effect of negative aerodynamic damping counteracts the effect of inherent damping of the structure, and the structure

continually absorbs energy from the wind field. Therefore, the amplitude of galloping increases with time; i.e., galloping occurs. Galloping can be prevented by increasing the inherent damping of the main cables in construction (e.g., utilization of vibration control ropes), which is an useful suggestion for engineers.

5. Conclusions

Both the CFD simulations and wind tunnel tests are used to study the galloping of steepled main cables for long-span suspension bridges during construction. To ensure accuracy of the results, the influences of the numerical model's grid size and the jaggy edges of the main cable's cross section on the numerical results are examined; and it is concluded that the numerical results are influenced by the jaggy edges of the main cable's cross section, and the influence cannot be ignored in the study of the onset of galloping based on the Den Hartog criterion. Experimental results of the main cable's aerodynamic coefficients are close to the corresponding numerical results, and both experimental and numerical studies reach the same conclusion on the onset of galloping. Numerical results show that all the six main cables in the different construction periods may suffer galloping based on the Den Hartog criterion, which is a possible explanation for the phenomenon of the large amplitude oscillation of steepled main cables during construction. Engineers should take some effective measures to control this harmful phenomenon due to the big possibility of the onset of the galloping during the construction period.

Acknowledgements

References

Assi, G.R.S. and Bearman, P.W. (2015), "Transverse galloping of circular cylinders fitted with solid and slotted splitter plates", *J. Fluid. Struct.*, **54**, 263-280.

An, Y.H., Spencer, B.F. and Ou, J.P. (2015), "A Test Method for Damage Diagnosis of Suspension Bridge Suspender Cables", *Comput. -Aided Civil Infrast. Eng.*, **30**, 771-784.

An, Y.H., Bartlomiej, B., Zhong, Y., Holobut, P. and Ou, J.P. (2016), "Rank-revealing QR decomposition applied to damage localization in truss structures", *Struct. Control Health Monit.*, DOI: 10.1002/stc.1849.

Blocken, B. and Toparlar, Y. (2015), "A following car influences cyclist drag: CFD simulations and wind tunnel measurements", *J. Wind Eng. Ind. Aerod.*, **145**, 178-186.

Cai, M.Q., Yan, B., Lu, X. and Zhou, L.S. (2015), "Numerical Simulation of Aerodynamic Coefficients of Iced-Quad Bundle Conductors". *IEEE T. Power Dilivery*, **30**(4), 1669-1676.

Den Hartog, J.P. (1932), "Transmission line vibration due to sleet", *Am. Inst. Elec. Engineers*, **51**(4), 1074-1081.

Franke, J., Hellsten, A., Schlünzen, H. and Carissimo, B. (2007), "Best Practice Guideline for the CFD

Simulation of Flows in the Urban Environment", *Proceedings of the COST Action732: Quality Assurance and Improvement of Microscale Meteorological Models*, Hamburg, Germany.

Holmes, J.D. (2015), *Wind Loading of Structures*, CRC Press.

Hu, G., Tse, K.T. and Kwok, K.C.S. (2015a), "Galloping of forward and backward inclined slender square cylinders", *J. Wind Eng. Ind. Aerod.*, **142**, 232-245.

Hu, G., Tse, K.T., Kwok, K.C.S. and Chen, Z.S. (2015b), "Pressure measurements on inclined square prisms", *Wind Struct.*, **21**,(4), 383-405.

Hu, J., Yan, B., Zhou, S., and Zhang, H.Y. (2012), "Numerical investigation on galloping of iced quad bundle conductors", *IEEE T. Power Dilivery*, **27**(2), 784-792.

Ibarra, D., Sorribes, F., Alonso, G. and Meseguer, J. (2014), "Transverse galloping of two-dimensional bodies having a rhombic cross-section", *J. Sound Vib.*, **333**, 2855-2865.

Jones, W.P. and Launder, B.E. (1972), "The prediction of laminarization with a two-equation model of turbulence", *Int. J. Heat Mass Transfer*, **15**(2), 301-314.

Kim, S. and Kim H.K. (2014), "Wake galloping phenomena between two parallel/unparallel cylinders", *Wind Struct.*, **18**(5), 511-528.

Li, S.L. and Ou, J.P. (2009), "Galloping analysis for the transient main cables of long-span suspension bridges during construction", *China Civil Eng. J.*, **42**(9), 74-81 (in Chinese).

Li, S.L., Wang, C.Q, Wang, D.W. and OU J.P. (2015a), "Galloping performance of large scale spire type main cable of suspension bridge during construction", *J. Vib. Shock*, **34**(22), 156-160 (in Chinese).

Li, S.L., Wang, F., An, Y.H. and Zheng, S.Y. (2015b), "Aerodynamic performance analysis of wind-sand flow on suspension bridge suspender cables", *Vibroengineering PROCEDIA*, 5, 537-541.

Macdonald, J.H.G. and Larose, G.L. (2007), "Two-degree-of-freedom inclined cable galloping-Part 1: General formulation and solution for perfectly tuned system", *J. Wind Eng. Ind. Aerod.*, **8**, 1-17.

Mannini, C., Marra, A.M. and Bartoli, G. (2014), "VIV-galloping instability of rectangular cylinders: Review and new experiments", *J. Wind Eng. Ind. Aerod.*, **132**, 109-124.

Pagnini, L.C., Freda, A. and Piccardo, G. (2016), "Uncertainties in the evaluation of one degree-of-freedom galloping onset", *European J. Environ. Civil Eng.*, 2016 (DOI: 10.1080/19648189.2016.1150900).

Païdoussis, M.P., Price, S.J. and deLangre, E. (2010), *Fluid-Structure Interactions: Cross-Flow-Induced Instabilities*, Cambridge University Press, .

Rezvani, M.A. and Mohebbi, M. (2014), "Numerical calculations of aerodynamic performance for ATM train at crosswind conditions", *Wind Struct.*, **18**(5), 529-548.

Tang Y., Zheng S.X. and Li M.S. (2015), "A numerical investigation on galloping of an inclined square cylinder in a smooth flow", *J. Wind Eng. Ind. Aerod.*, **144**(2015), 165-171.

Tse, K.T., Hu, G. and Kwok, K.C.S. (2014), "The effect of inclination on galloping of square cylinder and its mechanism", *Proceedings of the 7th International Symposium on Environmental Effects on Buildings and People: Actions, Influences, Interactions, Discomfort (EEBP VII)*, Cracow, Poland, October.

Wang, H., Li, A.Q. and Hu, R.M. (2011), "Comparison of ambient vibration response of the Runyang suspension bridge under skew winds with time-domain numerical predictions", *J. Bridge Eng.*, **16**(4), 513-526.

Wang, H., Li, A.Q., Niu, J., Zong, Z.H. and Li, J. (2013), "Long-term monitoring of wind characteristics at Sutong Bridge site", *J. Wind Eng. Ind. Aerod.*, **115**, 39-47.

Wang, Y.L. (1996), "Ground response of circular tunnel in poorly consolidated rock", *J. Geotech. Eng.*, **122**(9), 703-708.

Xin, D.B., Li, H., Wang, L. and Ou, J.P. (2012), "Experimental study on static characteristics of the bridge deck section under simultaneous actions of wind and rain", *J. Wind Eng. Ind. Aerod.*, **107-108**, 17-27.

Yan, B., Hu, J., Zhou, S. and Zhang, H.Y. (2011), "Anti-galloping for an iced quad-bundled conductor in stochastic wind field", *J. Vib. Shock*, **30**(7), 52-58 (in Chinese).

CC